PCCP

Accepted Manuscript

ROYAL SOCIETY OF CHEMISTRY

www.rsc.org/pccp

Spectral and Dynamical Properties of a Zr-Based MOF

Mario Gutiérrez,[1] Félix Sánchez[2] and Abderrazzak Douhal[1]*

[1]Departamento de Química Física, Facultad de Ciencias Ambientales y Bioquímica, INAMOL, Universidad de Castilla-La Mancha, Avenida Carlos III, S.N., 45071 Toledo, Spain.

[2] Instituto de Química Orgánica, CSIC, Juan de la Cierva, 3, 28006 Madrid, Spain.

*Corresponding author at Universidad de Castilla-La Mancha.

Tel.: +34 925 265 717; E-mail address: abderrazzak.douhal@uclm.es

Abstract

We report on the spectroscopy and dynamics of a Zr-naphthalene dicarboxylic acid (Zr-NDC) MOF in different diluted solvent suspensions and in a concentrated tetrahydrofuran (THF) one. In a diluted diethyl ether (DE) suspension, we observed intraparticle excimers formation between neighboring naphthalene organic linkers, leading to a red-shifted broad band in the emission spectrum and to a dynamics composed of three components of τ_1= 650 ps, τ_2= 3.7 ns and τ_3= 13.9 ns, assigned to the excimers photoproduction, monomers and excimers lifetimes, respectively. Furthermore, both absorption and emission spectra show a blue shift in more polar solvent characterized by the solvent polarity function f(ε,n). We also observed changes in the excimers formation time (490-840 ps) probably due to a variation in the MOF structural fluctuation induced by solvent filling. The global fluorescence quantum yield of these suspensions is around 0.30 ± 0.05. At higher concentrations of the MOF particles, we observed aggregates absorption and emission signals, having an intercrystal excimers formation in ~5 ps in a THF suspension, ~100 times shorter than the observed in a diluted one. Our results give the spectral and dynamical properties of a Zr-NDC MOF in solvent suspensions, opening the way to further studies of this kind of MOFs interacting with fluorescent dyes for possible photonics applications.

1. Introduction

During the latest two decades, research on the design of novel fluorescent nanomaterials with phototunable properties has aroused a great interest due to their applications in diverse fields of science and technology as nanophotonics or nanomedicine.[1, 2] Metal-Organic Framework (MOF) materials are one of the newest and promising nanomaterials for several applications. Owing to their excellent structural properties, like high specific surface areas, tunable cavity and related entrance volumes as well as their free and accessible cavities, MOFs have attracted considerable attention,[3, 4] as potential materials for a wide range of applications: chemical sensors,[5-10] optoelectronic devices,[11, 12] gas storage,[13-16] catalysis[17-19] and drug delivery,[20-23] to cite few of them. For example, recently, MIL-100 has used to photodeliver an antitumoral drug (Topotecan), using one or two photon excitations.[23] Thus, great progresses have been made to develop several kinds of MOFs containing specific ligands/metals and having different pore sizes, internal cavities and chemical structures.[4, 24, 25] While many contributions have demonstrated the use of MOFs in catalysis, gas storage and drug delivery, their luminescence properties are at the early stage of study and application.[26, 27] Because of their chemical structure (composed by metal nodes and organic linkers), their luminescence can originate from: 1) the metal nodes, 2) the organic ligands, 3) the interaction between the metal and organic ligand (Metal-to-Ligand charge transfer (MLCT) or Ligand-to-Metal charge transfer (LMCT)), 4) Antennae effects, or 5) excimer/exciplex due to photoevents between the ligands taking place in the excited state.[26] Several studies have focused on the photoluminescence properties of MOFs composed by lanthanide (Ln) ions as metal nodes. Their luminescence properties are governed by energy transfer (antennae effects) from the organic linkers to the metal nodes, and the emission spectra are characterized by narrow emission bands of Ln ions transitions.[28, 29] The use of the Ln-based MOFs for both sensing and white light emitting materials has been demonstrated.[6, 30, 31]

A large number of MOFs having the organic linker as the emissive part, is Zn-based,[32, 33] which have been proposed for sensing small molecules.[34, 35] For others metal-based MOFs, like $[Mg(DHT)(DMF)_2]_n$, the emission color, used as sensor of small molecules, depends on a proton-transfer process taking place in the organic linker.[36] BODIPY- and porphyrin-based MOFs (BOB and BOP) exhibit green and red emissions, respectively, from the organic ligand due to an energy transfer.[37] From the point of view of dynamics, only few studies in which the emission of excimers species due to the interaction between the MOF organic linkers have been reported.[32, 38]

On the other hand, owing to their nano- and micro-porous structure, MOFs can act as hosts for luminescent dyes opening the possibility to energy transfer (ET) photoevents in the formed host-guest hybrid complexes. These hybrid materials are proposed for energy harvesting,[39] detection of volatile organic compounds,[40, 41] organic photovoltaics,[42] and white light emitting devices (WLEDs).[12, 43]

Herein, we investigated the photodynamics of Zr-NDC in different solvent suspensions. For diluted suspensions, the interactions between the organic linkers of the same MOF nanoparticle lead to excimers formation in 490-840 ps and exhibit excimers emission with longer lifetimes (13-15 ns). Armed with the femtosecond (fs) spectroscopy we also studied the photodynamical behavior of a high concentrated Zr-NDC in a tetrahydrofuran (THF) suspension. We observed an ultrafast component (~5 ps) owing to the interaction between NDC linkers of neighboring MOF crystals. Our results shed light on the photobehavior of a Zr-NDC MOF in different solvent suspensions, paving the way to further investigations for possible photonics applications.

2. Experimental Section

Zr-NDC was prepared according to the procedures reported in the original references.[44, 45] X-ray diffraction (Bruker D8 diffractometer, Cu Kα radiation) was used to confirm the crystalline structure of the Zr-NDC. The synthesis method and corresponding analytical data are given in Electronic Supplementary Information (ESI†).

For the spectroscopic studies, the solvents (anhydrous): acetonitrile (ACN, 99.8%), dioxane (DO, 99.8%), tetrahydrofuran (THF, 99.9%), diethyl ether (DE, 99.9%) and dichloromethane (DCM, 99.9%) were from Sigma-Aldrich, and used as received. The diluted solvent suspensions were prepared by adding ~1 mg of Zr-NDC solid to ~20 mL of the solvent and sonicating during 15 minutes. The concentrated Zr-NDC in THF suspension was prepared by adding ~1 mg of Zr-NDC solid to ~1 ml of THF solvent and sonicating during 15 minutes.

The steady-state UV-visible absorption and fluorescence spectra have been recorded using JASCO V-670 and FluoroMax-4 (Jobin-Yvone) spectrophotometers, respectively. Fluorescence quantum yield of Zr-NDC suspensions in the used solvents were measured using an integrating sphere setup Quanta from Horiba coupled to FluoroMax-4 (Jobin-Yvone) spectrophotometer. To get scattering-free spectra of these suspensions, we have diluted the samples. Picosecond emission decays were measured using a time-correlated single-photon counting (TSCPC) system.[46] The samples were excited by a 40-ps pulsed diode laser centred

at 371 nm (<5 mW, 40 MHz repetition rate). The emission signal was collected at the magic angle and the instrument response function (IRF) was ~70 ps. The decays were deconvoluted and fitted to a multiexponential function using the FLUOFIT package (PicoQuant) allowing single and global fits. The quality of the fit was estimated by χ^2, which was always below 1.2.

The femtosecond (fs) emission transients have been collected using the fluorescence up-conversion technique. The system consists of a femtosecond Ti:sapphire oscillator (MaiTai HP, Spectra Physics) coupled to a second harmonic generation and up-conversion setups.[47] The oscillator pulses (90 fs, 250 mW, 80 MHz) were centered at 700, 720 or 740 nm and doubled in an optical setup through a 0.5-mm BBO crystal to generate a pumping beam at 350, 360 or 370 nm, respectively (~ 0.1 nJ). The polarization of the latter was set to magic angle in respect to the fundamental beam. The sample has been placed in a 1-mm thick rotating cell. The fluorescence was focused with reflective optics into a 1.0-mm BBO crystal and gated with the remaining fundamental fs-beam. The IRF of the full setup (measured as a Raman signal of pure solvent) was ~230 fs. To analyze the decays, a multiexponential function convoluted with the IRF was used to fit the experimental transients. All the experiments were performed at 293 K.

3. Results and Discussion

Figure 1 shows the SEM images, X-rays diffraction pattern, and a structural representation of Zr-NDC. Clearly, the sample is a highly crystalline material of an octahedral shape which edge is ≤ 400 nm. The structure (Figure 1D) contains two different internal cavities (a octahedral central cage with a pore size of ~14 Å surrounded by eight corner tetrahedral ones whose pores size is ~11 Å).[48] The topological structure shows a possible π-π interaction between the naphthalene rings. To explore the ligand-ligand interactions, we performed steady-state and ps-fs time-resolved emission studies of Zr-NDC in several diluted suspensions, and in a concentrated tetrahydrofuran (THF) one.

3.1. Zr-NDC Steady-State Absorption and Emission Spectra

To begin with, the UV-visible absorption and emission spectra of Zr-NDC compared to that of the organic linker (2,6-NDC) were recorded. Figure 2 A shows a comparison of the related spectra of both compounds in a diethyl ether (DE) suspension. Clearly, the absorption spectra for both systems are similar in shape (showing a vibrational structure, typical of

naphthalene derivatives) but that of Zr-NDC (0-0 transition at 357 nm) is shifted to longer wavelengths by 10 nm (800 cm^{-1}). The shift reflects the interaction between the organic linkers and the Zr-oxide cluster part.[48]

The emission spectrum of 2,6-NDC is a mirror-image of the absorption one (Figure 2 A). That of Zr-NDC is red shifted due to interactions between the naphthalenes and the Zr-oxide cluster parts, and exhibits a broader and red-shifted tail (around 450 nm). It is well known that naphthalenes at high concentrations or when they are embedded in polymeric matrixes form excimers (excited state dimers).[49-51] The excimers formation is reflected by a broader and red-shifted emission band, similar to the one observed in the Zr-NDC MOF spectrum. Therefore, we assign the broad emission band at 450 nm to excimers luminescence. Its intensity is not very high as it will depend on both excimers formation and fluorescence quantum yields. The excitation spectrum of Zr-NDC in a DE suspension does not depend on the observation wavelengths, indicating the same ground-state origin of the emitters. Considering that the closest carbon-carbon distance (~4 Å) between two adjacent naphthalene rings into the MOF (from X-Ray),[45] the excimers formation is topologically possible. In agreement with these observations, similar conformation of naphthalene molecules was observed for $[Fe_2(O)(O_2CCH_2C_{10}H_7)_2(TACN\text{-}Me_3)_2](PF_6)_2$ metal-organic complex, which exhibits a red-shifted emission band due to naphthalene excimers emission.[52] Different theoretical reports have investigated the singlet-singlet and triplet-triplet electronic states of naphthalene dimers in different conformations (face-to-face, T-shaped, etc), showing that the face-to-face (or eclipsed) conformation is the preferred one for the singlet state, leading to excimers.[53, 54] However, in the Zr-NDC MOF the naphthalenes linkers are interacting with Zr-metal nodes giving place to a three-dimensional network, which modifies the electronic coupling between the naphthalenes, changing the monomers dynamics and excimers formation photoproperties. To get information on the excimer photoproduction, the photodynamics of Zr-NDC was investigated and compared to that of 2,6-NDC.

3.2. Zr-NDC Picosecond Time-Resolved Emission Observations

Figure 2 B exhibits representative emission decays of Zr-NDC in a DE suspension observing at shorter (405 nm) and longer (500 nm) wavelengths, and upon excitation at 371 nm. Table 1 gives the obtained lifetime values together with the normalized (to 100) preexponential factors (a_i) and contributions ($c_i = \tau_i \times a_i$) using a global analysis procedure and multi-exponential model. While the decay of 2,6-NDC in DE exhibits a monoexponential behavior due to monomers emission (at low concentrations it does not form excimers), giving a single

fluorescence lifetime of 8.9 ns, that of Zr-NDC exhibits a rich behavior in which we observed decaying and rising components. At shorter emission wavelengths (≤ 440 nm): we got three decay times; τ_1= 650 ps, τ_2= 3.7 ns and τ_3= 13.9 ns, having the second component its maximum contribution at this region and opposite to the third one. However, for wavelengths longer than 470 nm, the τ_3-component presents its maximum contribution, while that of τ_2 has a very weak one, and τ_1 is now a rising signal. It is clear that 3.7 and 13.9 ns emitters share a common decaying and rising channel reflected in the τ_1 component. Thus, the 13.9 ns component is assigned to the excimer emission lifetime, the 3.7 ns corresponds to the monomer one, and the 650 ps is due to the excimer photoformation of closely naphthalene ligands. Comparable photodynamical behavior, in which the shorter component is assigned to the monomers and the longer one to the excimers, has been described for concentrated dimethyl-2,6-naphthalenedicarboxylate (2,6-NDC) in chloroform solutions.[49, 50] Time-resolved emission behavior of a highly concentrated (0.115 M) 2,6-NDC in a chloroform solution showed a biexponential behavior of 1.4 (assigned to the monomer species) and 15 ns (due to excimers ones), having the former its maximum contribution at the bluest part while the latter at the reddest one.[49] In a similar way, 2,6-NDC in a less concentrated chloroform solution (~10^{-2} M) exhibited a biexponential behavior with 6.8 (monomers lifetime) and 13.4 ns (excimers lifetime).[50] Moreover, the fluorescence decays of poly(polyoxy-tetramethylene-glycol naphthalene-2,6-dicarboxylate) (PTMN), even at lower concentration ($1.3x10^{-5}$ M), also showed a biexponential decay giving time constants of 3.6 and 10.2 ns, assigned to the monomers and excimers lifetimes, respectively.[49] To further investigate the photodynamics of the monomers in the Zr-NDC MOF, we have excited at 350 and observing at the bluest region (370 and 380 nm), where the emission is mainly from the MOF monomers. An accurate fit of the decays at these wavelengths, gating the signals within a 12-ns window, gives two lifetimes of 4.9 ns and 690 ps due to monomers emission and excimers formation, respectively.

3.3. Solvent Effect on Zr-NDC MOF

After understanding the Zr-NDC photobehavior in a DE suspension, we have explored the effect of solvent on the steady-state spectra and ps-photodynamics. Figure 3 displays normalized absorption and emission spectra together with the fluorescence decays at 500 nm upon excitation at 371 nm, using suspensions of acetonitrile (ACN), dioxane (DO), tetrahydrofuran (THF), diethyl ether (DE) and dichloromethane (DIC). Table 2 gives the obtained values of the emission decay parameters. The absorption spectra (Figure 3A) in the used solvents (except for DO) are similar in shape, showing a small shift to shorter

wavelengths with the solvent polarity function (f(ε,n); where ε and n are the dielectric constant and the refraction index, respectively). A comparable behavior is observed for the emission intensity maxima (Figure 3B), exhibiting a blue shift at higher values of f(ε,n) (Figure S1 in ESI†). However, both the absorption and emission spectra of the free linker, 2,6-NDC, do not show any simple correlation with f(ε,n) (Figure S2 in ESI†). Thus, we believe that the interaction between the naphthalene linkers and the Zr-metal cluster part in Zr-NDC is behind the hypsochromic behavior of Zr-NDC emission. Larger negative solvatochromism effects have been observed for other MOF-based systems as $((WS_4Cu_4)I_2(dptz)_3)\cdot DMF)_n$[55] and (Mg–NDI),[56] leading to their use as chemical sensor. On the other hand, the emission quantum yield of Zr-NDC in the used solvents is almost the same (0.30 ± 0.05). Focusing now on the ps-dynamics (Figure 3C and Figure S3 in ESI†), while the emission lifetimes of the monomers (τ_2=3.7-4.2 ns) and excimers (τ_3= 13.2-14.8 ns) present small changes with the solvent nature, the component corresponding with the excimers formation exhibits a significant change (τ_1= 490-840 ps) with the medium, reflecting the role of the environment on excimers formation (Table 2). We could not find any simple correlation between the values of τ_1 with the solvent polarity, acidity or basicity parameters. However, we suggest that a structure breathing of Zr-NDC MOF can happen by filling its pore with solvent molecules.[57] This lattice structural modification can alter the linker-linker distance, producing changes in the excimers formation, whose rate constant depends on the donor-acceptor distance and orientation. Recently ultrafast 2D IR spectroscopy has shown that filling the pores of a functionalized UiO-66 MOF with dimethylformamide leads to different structural fluctuations of the MOF,[58] substantially slowing down its dynamics. Other study on the so called a flexibility of MOF,[57, 59] reported on the structural lattice change in presence of trapped solvent into the cages.[60] In addition to that, another possible explanation of observing a solvent-dependent risetime of the excimers formation resides on the different dielectric constants of the used solvents (shielding effect) that could affect the electronic couplings between the 2,6-NDC linkers of the Zr-NDC MOF, modifying the energy transfer rate constant between the involved entities.

To conclude this part, Scheme 1 summarizes the above discussion of the photoevents taking place after the Zr-NDC photoexcitation in diluted suspensions. At S_1 the naphthalene monomers lead two different pathways: 1) they emit UV-blue light in 3.6-4.1 ns, and 2) they interact with other monomers at the ground state to form excimers in 490-840 ps, which emit blue light in 13-15 ns.

3.4. Femtosecond Observation

To explore the photobehaviour of Zr-NDC at higher concentration in the suspension, we have carried out both steady-state and fs-emission time-resolved measurements using highly concentrated Zr-NDC THF suspension (~1 mg / ml). Figure 4 exhibits the normalized absorption and emission spectra of a high concentrated Zr-NDC in THF suspension compared to those obtained for a diluted one, whereas Figure S4A (ESI†) shows the absorption spectrum of the concentrated sample (without normalize). While the absorption spectra are similar in shape, that of the concentrated sample displays a red-tail due to the interaction of closely MOFs nano-crystals (Figure 4A and Figure S4 A in ESI†). When exciting at 335 nm, the emission spectra are also similar in shape, but that of the concentrated sample is also red-shifted (Figure 4B). The shift is an indication of the particle interaction. Moreover, when exciting at 370 nm the concentrated sample, the emission spectrum is quite different, showing a broad band similar to that obtained for the Zr-NDC in solid-state (Figure 4B). The excitation spectrum of the concentrated sample (Figure S4 B in ESI†) also exhibits an increase in the intensity of the red-tail at longer observation wavelengths, indicating a major contribution of this population in the red-shifted emission signal. The appearance of the 380 nm absorption band in the excitation spectrum at higher Zr-NDC concentrations, and its absence in the spectrum of diluted sample reflect the aggregates (interparticle) absorption. Thus, the above observations indicate that at higher concentrations neighboring crystals of MOFs in suspensions strongly interact, showing red-shifted absorption and emission bands.

To get insight on the ultrafast photobehavior of the interacting closely crystals, we performed femtosecond (fs) time-resolved emission study in THF exciting at 350, 360 and 370 nm (Figure 4C). At the latter, we are mainly pumping the aggregates as said above (Figure 4A), while at 350 and 360 nm, both aggregated and non-aggregated MOF nanoparticles will be interrogated. Figure 4D shows the fs-emission transients upon excitation at 360 nm. In addition to the long sub-ns decaying and rising component observed in the ps-experiments (using diluted MOF suspensions), we got an ultrafast time (~5 ps) which is decaying at the bluest side of the spectra and rising at the reddest one. As said above, exciting at 360 nm will lead to excimers formation from monomers of the same crystals and from interacting ones. Thus, the observed dynamics is a combination of both intra as well as inter crystals interactions. To support this interpretation we also excited at different wavelengths (350 and 370 nm) and observed at 470 nm (Figure 4C). While the rising component exciting at 350 nm is 16 ps those upon exciting at 360 and 370 nm (the absorption is mainly due to the aggregated crystals) exhibit a substantial decrease being 5 and 3 ps, respectively. This observation clearly indicates that a component of 3 or 5 ps is mainly due to excimers

formation between closely MOF crystals. Note that the VR-cooling takes place in a similar time-scale than that observed here, so we cannot discard a contribution of the former to the obtained components. To check the possibility of a Zr-NDC photodegradation under fs-irradiation, we have taken the absorption spectra at different times (up to 15 min) using 350 nm fs-pulse laser beam. Figure S5 (ESI†) shows no significant spectral changes (in shape) suggesting that the fs-transient are free from a possible photodegradation.

To summarize this part, Scheme 2 displays a representation of the two different possibilities for the excimers photoformation, depending on the suspension concentration. In Zr-NDC diluted suspensions, the excimers photoformation takes place in 490-840 ps and it is mainly due to the interactions between naphthalenes of the same MOF nanoparticle. However, at higher concentrations the excimers are mostly formed in ~5 ps owing to the interactions between naphthalenes of neighboring MOF crystals.

4. Conclusion

Herein, we have reported on the spectral and photophysical properties of a Zr-NDC MOF in solvent suspensions, showing excimers formation between neighboring naphthalene linkers. The excimers formation is reflected by a broad red-shifted band in the Zr-NDC emission spectra and also by its dynamics, giving three components of τ_1= 650 ps (excimer formation process), τ_2= 3.7 ns (monomer lifetime) and τ_3= 13.9 ns (excimer lifetime). Increasing the polarity of the media, a blue shift in the emission spectra was observed. Moreover, while the monomer and excimer lifetimes do not exhibit much change with the medium, that of excimer photoformation shows a considerably change of almost twice (from 490 ps in ACN to 840 ps in DCM suspensions). We believe that the filling of the Zr-NDC pores with solvent molecules can lead to a structure breathing, modifying the linker-linker distance and therefore, producing changes in the excimers formation. At higher Zr-NDC concentrations, we observed an aggregation effect, reflected by a red-shift in the absorption and emission spectra. The fs-dynamics studies of the MOF in a concentrated THF suspension show an ultrafast component (~5 ps) assigned to the intercrystals excimers photoformations owing to the interaction between naphthalenes of closely MOF particles.

Our results give information on spectral and dynamical behaviors of Zr-NDC MOF in suspensions opening the way to further studies for future applications in photonics.

Acknowledgments

This work was supported by the MINECO through projects MAT2011-25472, MAT2014-52085-C2-2-P, Consolider Ingenio 2010 (CSD2009-0050, MULTICAT), and JCCM through preject PRI-PIBIN-2011-1283. M.G. thanks the MINECO for the Ph.D. Fellowship.

Electronic Supplementary Information (ESI†) Available: Figure S1 is a plot of the emission intensity maximum of Zr-NDC with the f (ε,n) of the solvent employed. Figure S2 gives the absorption and emission spectra of 2,6-NDC in the used solvents and a plot of the second emission peak spectral position with the f (ε,n) of the related solvents. Figure S3 shows the emission decays of Zr-NDC in some organic solvent suspensions exciting at 371 nm and observing at 405 nm. Figure S4 displays the absorption spectrum (without normalize) of a concentrated Zr-NDC THF suspension and the excitation spectra of Zr-NDC in diluted and concentrated THF suspensions. Figure S5 shows the absorption spectra of a concentrated Zr-NDC THF suspension upon fs-pulse laser beam irradiation at different times (up to 15 min). The synthesis, analytical and thermal gravimetric data are included in this part.

References:

1. W. Zheng; P. Huang; D. Tu; E. Ma; H. Zhu; X. Chen, Lanthanide-doped upconversion nano-bioprobes: electronic structures, optical properties, and biodetection. *Chem. Soc. Rev.* 2015**, 44** (6), 1379-1415.
2. G. Chen; H. Agren; T. Y. Ohulchanskyy; P. N. Prasad, Light upconverting core-shell nanostructures: nanophotonic control for emerging applications. *Chem. Soc. Rev.* 2015**, 44** (6), 1680-1713.
3. Special Issue on Metal-Organic Framework. *Chem. Rev. (Washington, DC, U. S.)* 2012**, 112** (2), 673-1268.
4. H. Furukawa; K. E. Cordova; M. O'Keeffe; O. M. Yaghi, The Chemistry and Applications of Metal-Organic Frameworks. *Science* 2013**, 341** (6149).
5. W. Liu; T. Jiao; Y. Li; Q. Liu; M. Tan; H. Wang; L. Wang, Lanthanide Coordination Polymers and Their Ag+-Modulated Fluorescence. *J. Am. Chem. Soc.* 2004**, 126** (8), 2280-2281.
6. B. Chen; Y. Yang; F. Zapata; G. Lin; G. Qian; E. B. Lobkovsky, Luminescent Open Metal Sites within a Metal–Organic Framework for Sensing Small Molecules. *Adv. Mater. (Weinheim, Ger.)* 2007**, 19** (13), 1693-1696.
7. Z. Xie; L. Ma; K. E. deKrafft; A. Jin; W. Lin, Porous Phosphorescent Coordination Polymers for Oxygen Sensing. *J. Am. Chem. Soc.* 2009**, 132** (3), 922-923.
8. Y. Takashima; V. M. Martínez; S. Furukawa; M. Kondo; S. Shimomura; H. Uehara; M. Nakahama; K. Sugimoto; S. Kitagawa, Molecular decoding using luminescence from an entangled porous framework. *Nature Communications* 2011**, 2** (1).
9. C. Zhang; Y. Che; Z. Zhang; X. Yang; L. Zang, Fluorescent nanoscale zinc(ii)-carboxylate coordination polymers for explosive sensing. *Chem. Commun. (Cambridge, U. K.)* 2011**, 47** (8), 2336-2338.
10. L. E. Kreno; K. Leong; O. K. Farha; M. Allendorf; R. P. Van Duyne; J. T. Hupp, Metal–Organic Framework Materials as Chemical Sensors. *Chem. Rev. (Washington, DC, U. S.)* 2011**, 112** (2), 1105-1125.
11. M. Alvaro; E. Carbonell; B. Ferrer; F. X. Llabrés i Xamena; H. Garcia, Semiconductor Behavior of a Metal-Organic Framework (MOF). *Chemistry – A European Journal* 2007**, 13** (18), 5106-5112.
12. C. Y. Sun; X. L. Wang; X. Zhang; C. Qin; P. Li; Z. M. Su; D. X. Zhu; G. G. Shan; K. Z. Shao; H. Wu; J. Li, Efficient and tunable white-light emission of metal-organic frameworks by iridium-complex encapsulation. *Nature Communications* 2013**, 4**.
13. N. L. Rosi; J. Eckert; M. Eddaoudi; D. T. Vodak; J. Kim; M. O'Keeffe; O. M. Yaghi, Hydrogen Storage in Microporous Metal-Organic Frameworks. *Science* 2003**, 300** (5622), 1127-1129.
14. A. R. Millward; O. M. Yaghi, Metal−Organic Frameworks with Exceptionally High Capacity for Storage of Carbon Dioxide at Room Temperature. *J. Am. Chem. Soc.* 2005**, 127** (51), 17998-17999.
15. O. K. Farha; A. Ö. Yazaydin; I. Eryazici; C. D. Malliakas; B. G. Hauser; M. G. Kanatzidis; S. T. Nguyen; R. Q. Snurr; J. T. Hupp, De novo synthesis of a metal-organic framework material featuring ultrahigh surface area and gas storage capacities. *Nature Chem.* 2010**, 2** (11), 944-948.
16. S. Ma; H.-C. Zhou, Gas storage in porous metal-organic frameworks for clean energy applications. *Chem. Commun. (Cambridge, U. K.)* 2010**, 46** (1), 44-53.
17. F. X. Llabrés i Xamena; A. Abad; A. Corma; H. Garcia, MOFs as catalysts: Activity, reusability and shape-selectivity of a Pd-containing MOF. *J. Catal.* 2007**, 250** (2), 294-298.
18. L. Ma; C. Abney; W. Lin, Enantioselective catalysis with homochiral metal-organic frameworks. *Chem. Soc. Rev.* 2009**, 38** (5), 1248-1256.

19. J.-y. Ye; C.-j. Liu, Cu3(BTC)2: CO oxidation over MOF based catalysts. *Chem. Commun. (Cambridge, U. K.)* 2011**, 47** (7), 2167-2169.
20. P. Horcajada; C. Serre; M. Vallet-Regí; M. Sebban; F. Taulelle; G. Férey, Metal–Organic Frameworks as Efficient Materials for Drug Delivery. *Angew. Chem.* 2006**, 118** (36), 6120-6124.
21. P. Horcajada; C. Serre; G. Maurin; N. A. Ramsahye; F. Balas; M. Vallet-Regí; M. Sebban; F. Taulelle; G. Férey, Flexible Porous Metal-Organic Frameworks for a Controlled Drug Delivery. *J. Am. Chem. Soc.* 2008**, 130** (21), 6774-6780.
22. J. Della Rocca; D. Liu; W. Lin, Nanoscale Metal–Organic Frameworks for Biomedical Imaging and Drug Delivery. *Acc. Chem. Res.* 2011**, 44** (10), 957-968.
23. M. R. di Nunzio; V. Agostoni; B. Cohen; R. Gref; A. Douhal, A "Ship in a Bottle" Strategy To Load a Hydrophilic Anticancer Drug in Porous Metal Organic Framework Nanoparticles: Efficient Encapsulation, Matrix Stabilization, and Photodelivery. *J. Med. Chem.* 2013**, 57** (2), 411-420.
24. J. L. C. Rowsell; O. M. Yaghi, Metal–organic frameworks: a new class of porous materials. *Microporous Mesoporous Mater.* 2004**, 73** (1–2), 3-14.
25. T. R. Cook; Y.-R. Zheng; P. J. Stang, Metal–Organic Frameworks and Self-Assembled Supramolecular Coordination Complexes: Comparing and Contrasting the Design, Synthesis, and Functionality of Metal–Organic Materials. *Chem. Rev. (Washington, DC, U. S.)* 2013**, 113** (1), 734-777.
26. M. D. Allendorf; C. A. Bauer; R. K. Bhakta; R. J. T. Houk, Luminescent metal-organic frameworks. *Chem. Soc. Rev.* 2009**, 38** (5), 1330-1352.
27. Y. Cui; Y. Yue; G. Qian; B. Chen, Luminescent Functional Metal–Organic Frameworks. *Chem. Rev. (Washington, DC, U. S.)* 2011**, 112** (2), 1126-1162.
28. M. O. Rodrigues; F. A. A. Paz; R. O. Freire; G. F. de Sá; A. Galembeck; M. C. B. S. M. Montenegro; A. N. Araújo; S. Alves, Modeling, Structural, and Spectroscopic Studies of Lanthanide-Organic Frameworks. *The Journal of Physical Chemistry B* 2009**, 113** (36), 12181-12188.
29. X. Yan; Z. Cai; C. Yi; W. Liu; M. Tan; Y. Tang, Anion-Induced Structures and Luminescent Properties of Chiral Lanthanide−Organic Frameworks Assembled by an Achiral Tripodal Ligand. *Inorg. Chem.* 2011**, 50** (6), 2346-2353.
30. Z. Guo; H. Xu; S. Su; J. Cai; S. Dang; S. Xiang; G. Qian; H. Zhang; M. O'Keeffe; B. Chen, A robust near infrared luminescent ytterbium metal-organic framework for sensing of small molecules. *Chem. Commun. (Cambridge, U. K.)* 2011**, 47** (19), 5551-5553.
31. S. Dang; J.-H. Zhang; Z.-M. Sun, Tunable emission based on lanthanide(iii) metal-organic frameworks: an alternative approach to white light. *J. Mater. Chem.* 2012**, 22** (18), 8868-8873.
32. C. A. Bauer; T. V. Timofeeva; T. B. Settersten; B. D. Patterson; V. H. Liu; B. A. Simmons; M. D. Allendorf, Influence of Connectivity and Porosity on Ligand-Based Luminescence in Zinc Metal−Organic Frameworks. *J. Am. Chem. Soc.* 2007**, 129** (22), 7136-7144.
33. X. Li; X.-W. Wang; Y.-H. Zhang, Blue photoluminescent 3D Zn(II) metal-organic framework constructing from pyridine-2,4,6-tricarboxylate. *Inorg. Chem. Commun.* 2008**, 11** (8), 832-834.
34. B. Chen, Isoreticular metal-organic framework of the formula Zn4O(FMA)3. US patent 8597406 B2: 2013.
35. B. Chen; Z. Zhang, Zn4(OH)2(1,2,4-BTC)2—a rod packing microporous metal-organic framework with open metal sites for selective separation and sensing of small molecules. US8507406 B2: 2013.
36. K. Jayaramulu; P. Kanoo; S. J. George; T. K. Maji, Tunable emission from a porous metal-organic framework by employing an excited-state intramolecular proton transfer responsive ligand. *Chem. Commun. (Cambridge, U. K.)* 2010**, 46** (42), 7906-7908.

37. C. Y. Lee; O. K. Farha; B. J. Hong; A. A. Sarjeant; S. T. Nguyen; J. T. Hupp, Light-Harvesting Metal–Organic Frameworks (MOFs): Efficient Strut-to-Strut Energy Transfer in Bodipy and Porphyrin-Based MOFs. *J. Am. Chem. Soc.* 2011**, 133** (40), 15858-15861.
38. C.-C. Wang; C.-C. Yang; W.-C. Chung; G.-H. Lee; M.-L. Ho; Y.-C. Yu; M.-W. Chung; H.-S. Sheu; C.-H. Shih; K.-Y. Cheng; P.-J. Chang; P.-T. Chou, A New Coordination Polymer Exhibiting Unique 2D Hydrogen-Bonded (H2O)16 Ring Formation and Water-Dependent Luminescence Properties. *Chemistry – A European Journal* 2011**, 17** (33), 9232-9241.
39. H. C. Streit; M. Adlung; O. Shekhah; X. Stammer; H. K. Arslan; O. Zybaylo; T. Ladnorg; H. Gliemann; M. Franzreb; C. Wöll; C. Wickleder, Surface-Anchored MOF-Based Photonic Antennae. *ChemPhysChem* 2012**, 13** (11), 2699-2702.
40. D. Yan; Y. Tang; H. Lin; D. Wang, Tunable Two-color Luminescence and Host-guest Energy Transfer of Fluorescent Chromophores Encapsulated in Metal-Organic Frameworks. *Sci. Rep.* 2014**, 4**.
41. M.-J. Dong; M. Zhao; S. Ou; C. Zou; C.-D. Wu, A Luminescent Dye@MOF Platform: Emission Fingerprint Relationships of Volatile Organic Molecules. *Angewandte Chemie International Edition* 2014**, 53** (6), 1575-1579.
42. K. Leong; M. E. Foster; B. M. Wong; E. D. Spoerke; D. Van Gough; J. C. Deaton; M. D. Allendorf, Energy and charge transfer by donor-acceptor pairs confined in a metal-organic framework: a spectroscopic and computational investigation. *Journal of Materials Chemistry A* 2014**, 2** (10), 3389-3398.
43. Dye/metal-organic framework composite material for white light emission and preparation method thereof. CN patent 103740361: 2014.
44. A. Schaate; P. Roy; A. Godt; J. Lippke; F. Waltz; M. Wiebcke; P. Behrens, Modulated Synthesis of Zr-Based Metal–Organic Frameworks: From Nano to Single Crystals. *Chemistry – A European Journal* 2011**, 17** (24), 6643-6651.
45. V. Bon; I. Senkovska; M. S. Weiss; S. Kaskel, Tailoring of network dimensionality and porosity adjustment in Zr- and Hf-based MOFs. *CrystEngComm* 2013**, 15** (45), 9572-9577.
46. J. A. Organero; L. Tormo; A. Douhal, Caging ultrafast proton transfer and twisting motion of 1-hydroxy-2-acetonaphthone. *Chem. Phys. Lett.* 2002**, 363** (3–4), 409-414.
47. M. Gil; A. Douhal, Femtosecond Dynamics in Ionic Structures of a Heart Medicine. *Chem. Phys. Lett.* 2006**, 432** (1–3), 106-109.
48. W. Zhang; H. Huang; D. Liu; Q. Yang; Y. Xiao; Q. Ma; C. Zhong, A new metal–organic framework with high stability based on zirconium for sensing small molecules. *Microporous Mesoporous Mater.* 2013**, 171** (0), 118-124.
49. T. Cao; X. Zhang; R. Qian, Excimer fluorescence of poly(polyoxytetramethylene-glycol naphthalene-2,6-dicarboxylate). *Polym. J. (Tokyo, Jpn.)* 1989**, 21** (6), 489-497.
50. C. Spies; R. Gehrke, Time-resolved fluorescence measurements on solutions of dimethyl-2,6-naphthalenedicarboxylate. *J. Lumin.* 1999**, 82** (4), 333-340.
51. C. Spies; R. Gehrke, Excimer Formation of Dimethyl 2,6-Naphthalene Dicarboxylate Embedded in a Poly(methyl methacrylate) Matrix. *The Journal of Physical Chemistry A* 2002**, 106** (21), 5348-5352.
52. L. B. Picraux; B. T. Weldon; J. K. McCusker, Intramolecular Excimer Formation in a Naphthalene-Appended Dinuclear Iron−Oxo Complex. *Inorg. Chem.* 2003**, 42** (2), 273-282.
53. A. L. L. East; E. C. Lim, Naphthalene dimer: Electronic states, excimers, and triplet decay. *The Journal of Chemical Physics* 2000**, 113** (20), 8981-8994.
54. M. Pabst; B. Lunkenheimer; A. Köhn, The Triplet Excimer of Naphthalene: A Model System for Triplet−Triplet Interactions and Its Spectral Properties. *The Journal of Physical Chemistry C* 2011**, 115** (16), 8335-8344.

55. Z.-Z. Lu; R. Zhang; Y.-Z. Li; Z.-J. Guo; H.-G. Zheng, Solvatochromic Behavior of a Nanotubular Metal−Organic Framework for Sensing Small Molecules. *J. Am. Chem. Soc.* 2011**, 133** (12), 4172-4174.
56. A. Mallick; B. Garai; M. A. Addicoat; P. S. Petkov; T. Heine; R. Banerjee, Solid state organic amine detection in a photochromic porous metal organic framework. *Chemical Science* 2015**, 6** (2), 1420-1425.
57. G. Ferey; C. Serre, Large breathing effects in three-dimensional porous hybrid matter: facts, analyses, rules and consequences. *Chem. Soc. Rev.* 2009**, 38** (5), 1380-1399.
58. J. Nishida; A. Tamimi; H. Fei; S. Pullen; S. Ott; S. M. Cohen; M. D. Fayer, Structural dynamics inside a functionalized metal–organic framework probed by ultrafast 2D IR spectroscopy. *Proceedings of the National Academy of Sciences* 2014**, 111** (52), 18442-18447.
59. Z. Wang; S. M. Cohen, Modulating Metal−Organic Frameworks To Breathe: A Postsynthetic Covalent Modification Approach. *J. Am. Chem. Soc.* 2009**, 131** (46), 16675-16677.
60. S. Horike; S. Shimomura; S. Kitagawa, Soft porous crystals. *Nat Chem* 2009**, 1** (9), 695-704.

Captions of figures and tables

Scheme 1. Proposed mechanisms for the photoprocesses taking place within Zr-NDC MOF in the used diluted solvent suspensions after the photoexcitation. M* and (MM*) are the excited monomers and excimers, respectively.

Scheme 2. Representation of the excimers photoformation in A) Diluted suspensions, due to interaction between naphthalenes of the same MOF crystal; and B) Concentrated THF suspension, owing to interactions between naphthalenes of closely MOF crystals.

Figure 1. (A), (B) Scanning Electron Microscopy (SEM) images of Zr-NDC crystals. (C) X-ray diffraction spectrum of Zr-NDC (Bruker D8 diffractometer, Cu Kα radiation). (D) Illustration of the Zr-NDC MOF crystalline structure (Zr polyhedron is represented by blue, O by red atoms, C by black and H by grey). The yellow spheres indicate the tetrahedral cages while the green ones those of the octahedral pores.

Figure 2. (A) Normalized UV-visible absorption and emission spectra of 2,6-NDC (black dashed line) and Zr-NDC (red solid line) in DE suspensions. For emission the excitation wavelength was 335 nm. (B) Magic-angle emission decays of Zr-NDC (blue and red, respectively) in DE suspensions. The observation wavelength is indicated as inset and the samples were excited at 371 nm. The solid lines are from the best-fit using a multiexponential function and the IRF is the instrumental response function.

Figure 3. Normalized UV-visible (A) absorption and (B) fluorescence spectra of Zr-NDC in (1) ACN (black line), (2) THF (red line), (3) DE (dark yellow line), (4) DO (blue line) and (5) DIC (green line) suspensions. For emission, the excitation wavelength was 335 nm. (C) Magic-angle emission decays of Zr-NDC in (1) ACN (red), (2) THF (green), (3) DO (blue), (4) DE (grey) and (5) DIC (pink) suspensions. The samples were excited at 371 nm and the observation wavelength was 500 nm. The solid lines are from the best-fit using a multiexponential function and the IRF is the instrumental response function.

Figure 4. Normalized UV-visible (A) absorption spectra of diluted (~1mg / 20mL, dashed line) and concentrated (~1mg / mL, solid line) Zr-NDC THF suspensions; and (B) emission spectra of a diluted (black dashed line, λ_{exc} = 335 nm) and concentrated (red solid line and blue dotted line λ_{exc} =335 and 370 nm, respectively) Zr-NDC THF suspensions, and Zr-NDC

in solid-state (green dashed-dotted line, λ_{exc} = 350 nm). Fs-emission transients of high concentrated Zr-NDC THF suspension exciting at (C) 350, 360 and 370 nm and observing at 470 nm, and (D) exciting at 360 nm and observing as indicated. The solid lines are from the best multiexponential fits.

Table 1. Values of time constants (τ_i), normalized (to 100) pre-exponential factors (a_i) and fractional contributions ($c_i = \tau_i a_i$) obtained from the fit of the emission decays of Zr-NDC in a DE suspension upon excitation at 371 nm and observation as indicated. The negative sign for a_1 indicates a rising component in the emission signal. The error estimation is provided by the fluofit analysis of the decay.

Table 2. Values of time constants (τ_i) obtained from the global fit of the emission decays of Zr-NDC in the used solvents, upon excitation at 371 nm and observation as indicated. The error estimation is provided by the fluofit analysis of the decay.

Scheme 1.

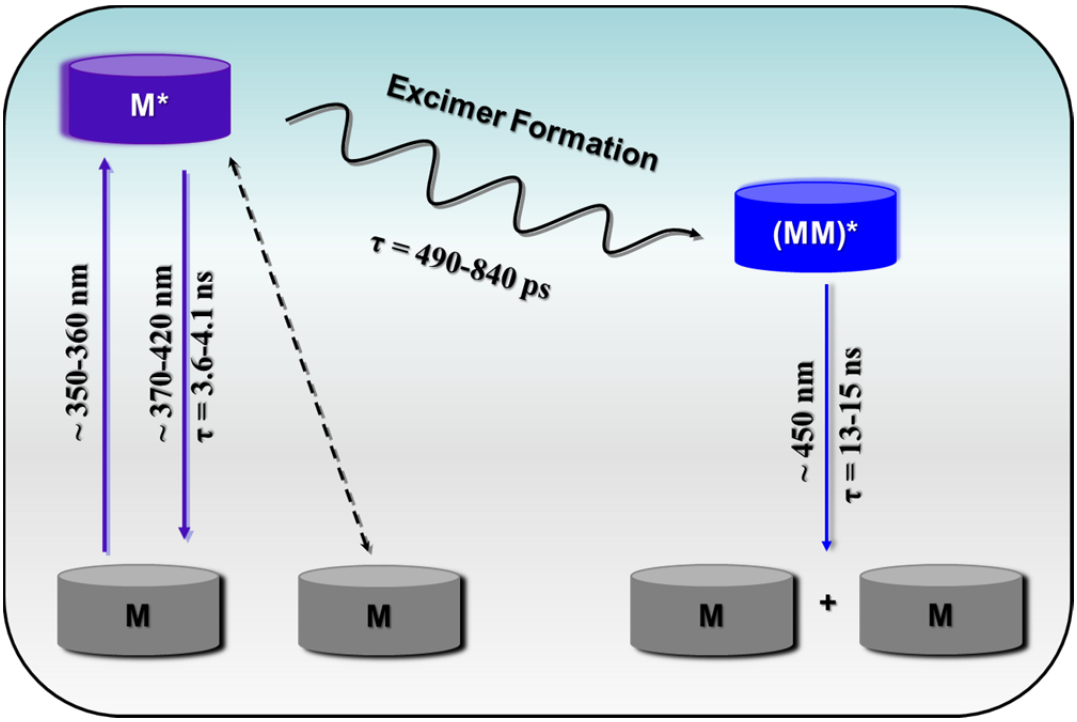

Scheme 2.

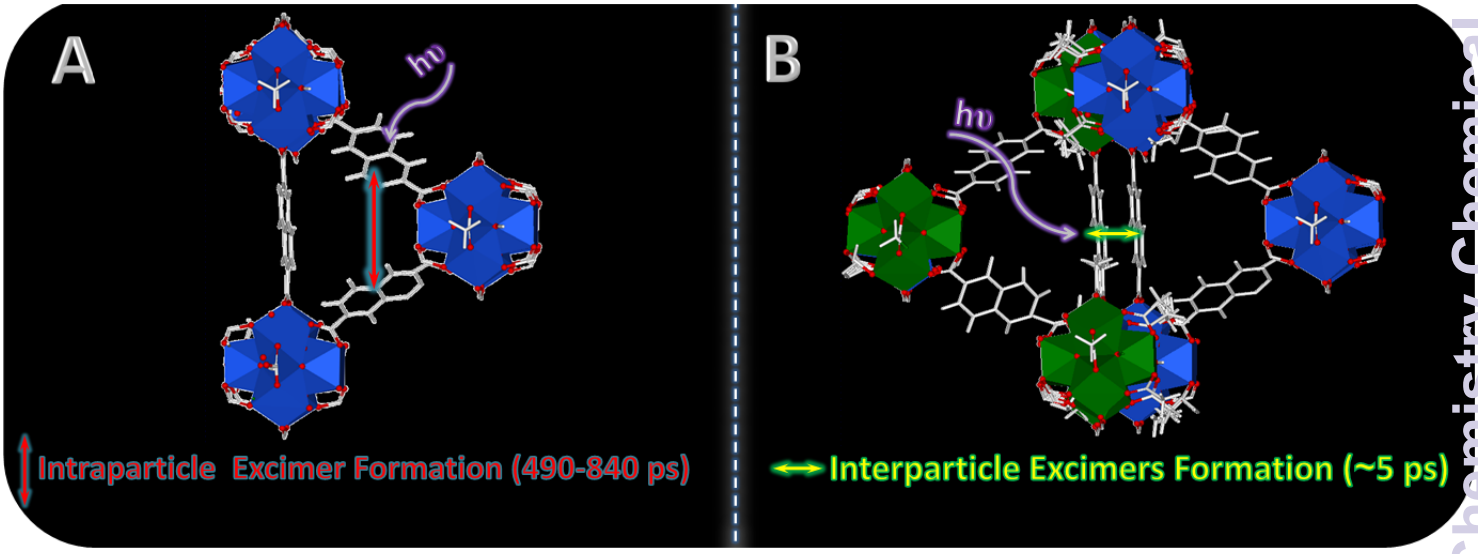

Figure 1.

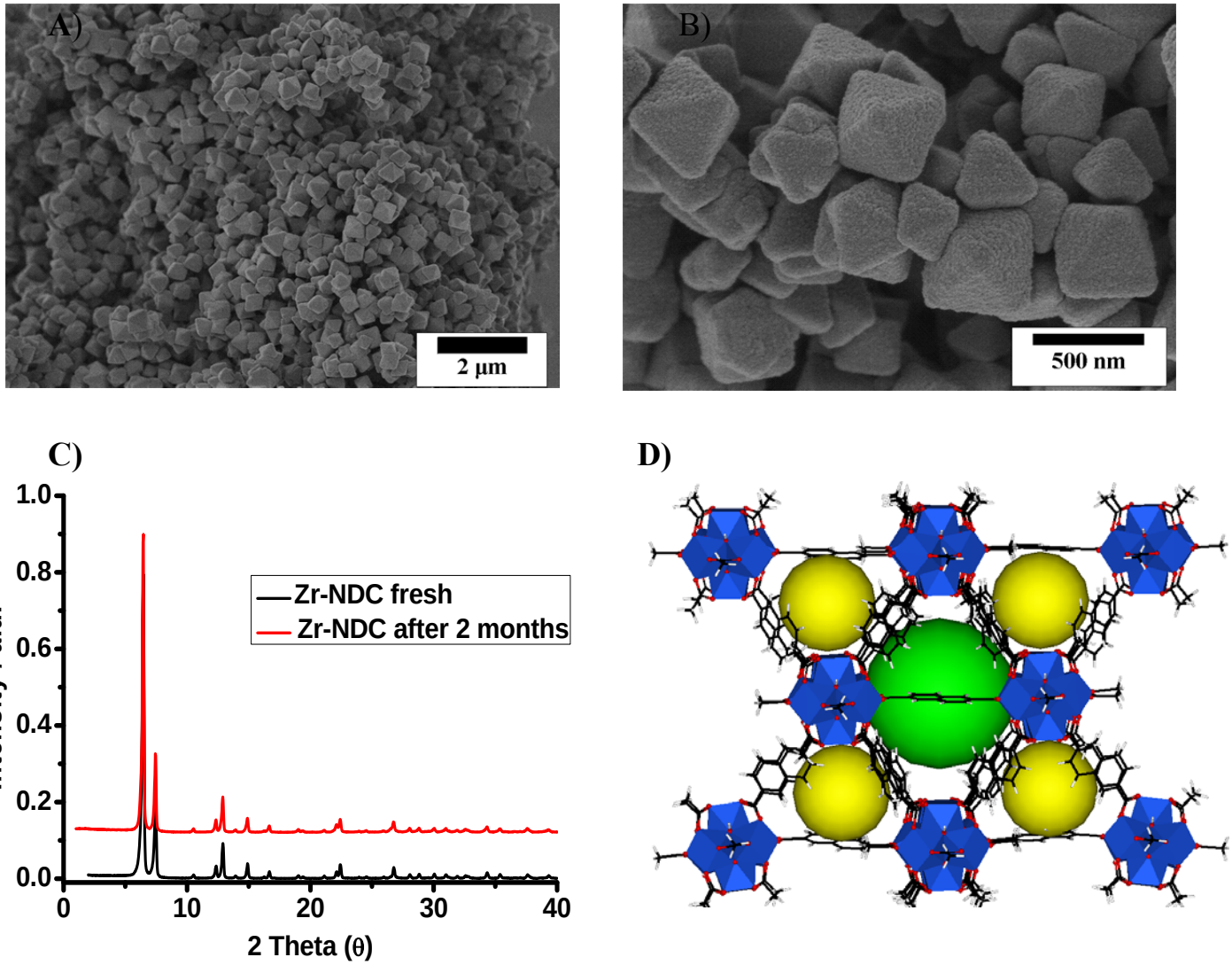

Figure 2.

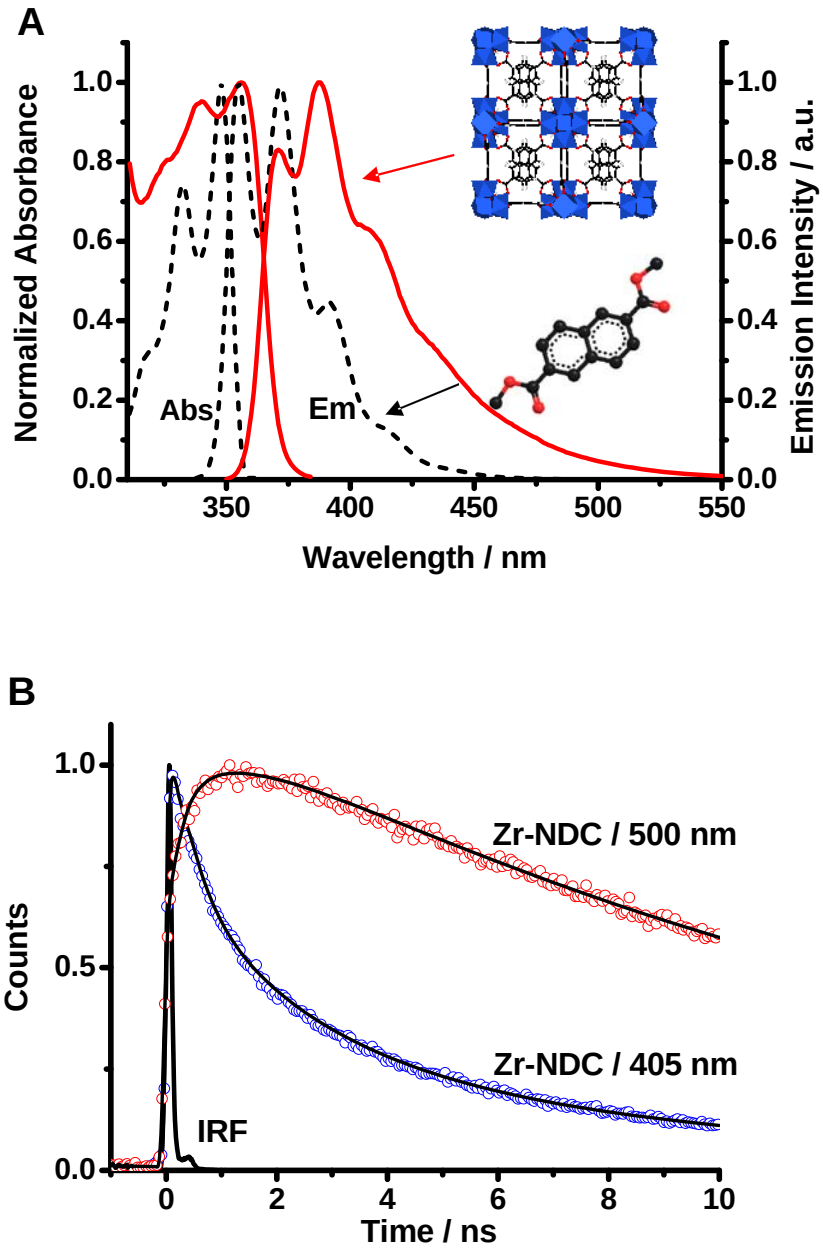

Figure 3.

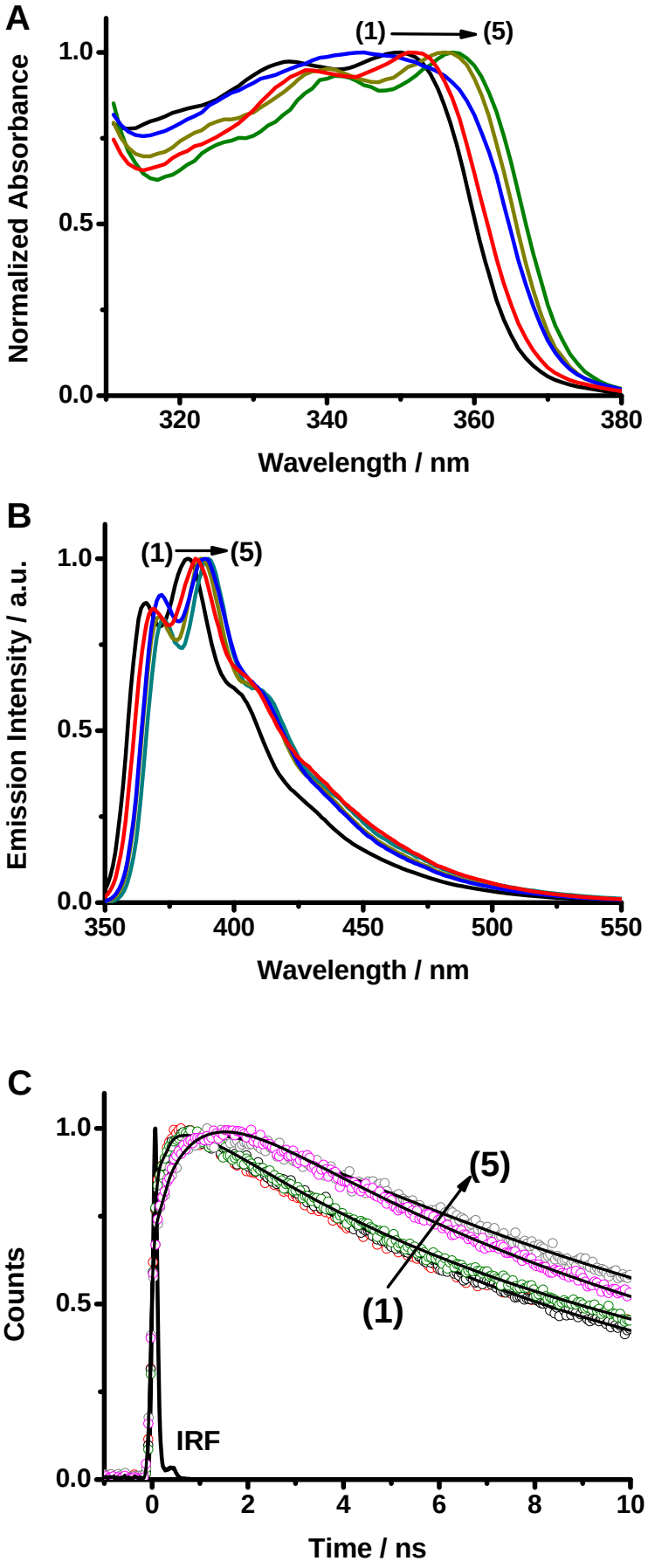

Figure 4.

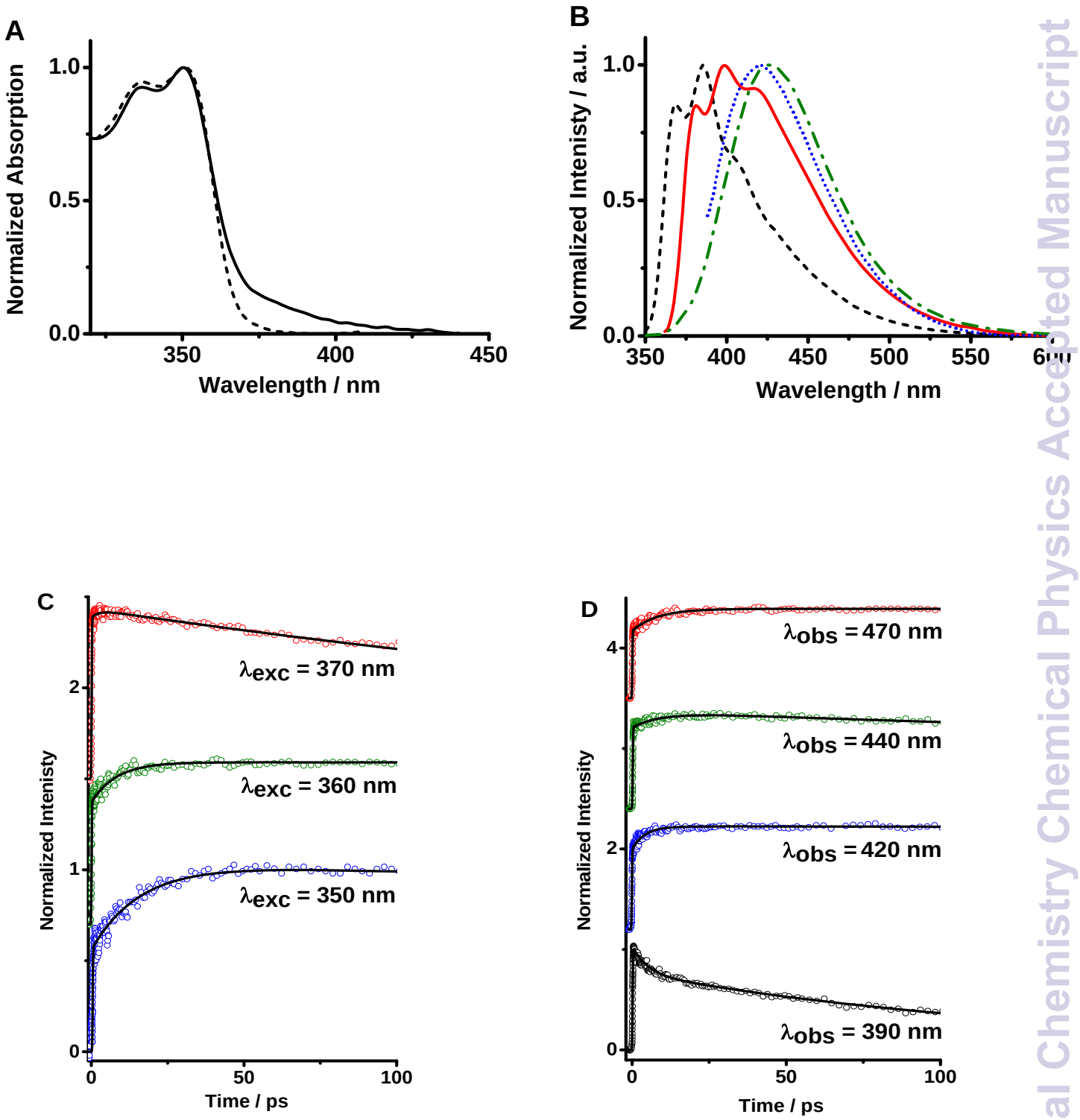

Table 1.

λ obs (nm)	τ_1 / ps ± 50	a_1	c_1	τ_2 / ns ± 0.2	a_2	c_2	τ_3 / ns ± 0.3	a_3	c_3
405	650	45	8	3.7	40	38	13.9	15	54
435	650	40	5	3.7	35	26	13.9	25	69
475	650	-100	-100	3.7	18	6	13.9	82	94
500	650	-100	-100	3.7	15	5	13.9	85	95
525	650	-100	-100	3.7	10	3	13.9	90	97

Table 2.

Solvent	τ_1 / ps (*) ± 50	τ_2 / ns ± 0.2	τ_3 / ns ± 0.3
Acetonitrile	490	3.9	14.3
Dioxane	550	4.3	13.5
Tetrahydrofuran	620	4.4	14.8
Diethyl Ether	650	3.7	13.9
Dichloromethane	840	4.2	13.2

(*) Decay at the blue (405-435 nm), while it is a rise at the red (475-525 nm) regions.